I'm listening ...

Samareh Attarsharghi

Attarsharghi combines laboratory testing with simulation and theoretical analysis to arrive at a practical approach to measuring ocean currents over large areas based on a call-response network of acoustic transducers.

Who should read this paper?

All those with an interest in ocean currents, underwater acoustics and the practical aspects of deploying an underwater acoustic sensor network.

Why is it important?

Of all of the physical parameters of the ocean realm, the speed and direction of the movement of ocean water, otherwise referred to as ocean "current," is one of the most problematic to characterize. Point measurements are relatively easy to make using widely available, robust current meter technology. Over time, these point measurements can reveal current patterns at the measurement location. But real-time characterization of the complex movements of shallow ocean water masses over broad areas remains a bit of a "holy grail" for scientists and ocean industry alike. And yet currents carry vital nutrients for fish, govern the movements of icebergs, describe ever-changing ribbons of constant temperature or salinity, and can either work against or with the movement of ships at sea. As such, the understanding of ocean currents over space and time is of practical importance to both ocean enterprise and research alike.

In the wonderful world of oceanography, ocean currents are typically grouped into "surface" currents (the upper 400 m that comprise roughly 10% of the oceans) and "deep water" currents (the remaining 90% of ocean waters deeper than 400 m). Deep water currents are driven by gravity acting on variations in water density – which is a function of differences in temperature and salinity – while surface currents are also influenced by solar heating and winds.

In this paper, the author tackles the theoretical and practical aspects of a broad area ocean current measurement system that uses acoustic transducers – devices that transmit and receive pulses of sound. Her innovative ideas are first tested in a lab-scale prototype, which helped in understanding some of the practical challenges. Observations made in the lab were then incorporated into a large-scale system design and deployment strategy for the Northwest Atlantic. Simulation was then used to test the effectiveness of the large-scale system design. The work focused in particular on finding the optimal positioning of the acoustic transducers to minimize multipath effect created by variations in both temperature and salinity – themselves the engines of ocean currents.

About the author

Samareh Attarsharghi is a doctoral candidate at Memorial University of Newfoundland. Her area of study is underwater acoustic sensor networks. She is currently developing new architectures of acoustic sensor networks for ocean current monitoring which are optimized to minimize both energy consumption and inherent measurement errors.

DESIGN CRITERIA AND PRACTICAL INSIGHTS INTO AN UNDERWATER CURRENT MEASUREMENT SYSTEM ALONG WITH SIMULATION RESULTS OF A REAL-CASE SCENARIO IN THE NORTHWEST ATLANTIC OCEAN

Samareh Attarsharghi

Faculty of Engineering and Applied Science, Memorial University of Newfoundland, St. John's, NL, Canada

ABSTRACT

Acoustics have been used in underwater communication and environmental sensing for a century. Sound waves propagate well in water; however, the marine environment poses many challenges to this phenomenon. Designing and deploying an underwater acoustic sensor network has always been a challenge due to the inhomogeneity of the propagation medium. In this paper, a background theory of the underwater sound propagation is provided followed by practical observations and insights into innovative ideas achieved in a lab-scale prototype which assisted in overcoming these challenges. These observations are used to propose a large-scale deployment strategy in the Northwest Atlantic region. Bellhop simulation results provide evidence of the effectiveness of a large-scale system design. This work is focused on finding optimal positioning of the acoustic sensors in the sea while minimizing the multipath effect at the receiver. In addition, the process for precise current speed measurement in a laboratory environment has been explained which elaborates on the practical aspects of a large-scale network deployment in the ocean. The Doppler effect, caused by the motion of the transducers due to wave motion in the sea, is also considered and analyzed for signal processing needs.

INTRODUCTION

Monitoring the marine environment is a subject of interest to many businesses including offshore and shipping industries. As icebergs are a threat in the North Atlantic region, many researchers have tried to propose solutions to minimize the risk of iceberg collisions. Among these solutions, iceberg trajectory modelling such as Turnbull et al. [2015] and Eik [2009] are examples of iceberg drift predictions so that the related industries manage to avoid collisions.

According to Eik [2009] currents, specifically, are the most important factor for iceberg drift modelling. Eik also mentions a poor quality of available current velocity data for his model. The importance of a robust real-time in-situ current data is reinforced in Turnbull et al. [2015] as they also had difficulty in modelling and collecting data for their iceberg forecasting operation. Thus, it is extremely important to monitor and measure the velocity of the current accurately, as the precise sets of current data provide researchers the ability to model and predict the trajectory of icebergs.

Urick [1983] reports that the onset of the interest in using underwater acoustics and sonar waves in detecting icebergs was in the early 20th century. Later on, acoustic waves were used to detect submarines or other applications including data communication for ocean monitoring [Groen et al., 2001; Gough and Hawkins, 1998; and Chapman et al., 1999]. Acoustic waves have also been used for ocean monitoring and current measurements. There are a number of methods to measure the currents in the ocean that can be grouped into two major categories. The first category is remote sensing techniques, such as radars [Paduan and Graber, 1997]. This technique only measures the surface ocean current and not the current at the desired depth. Examples include the National Oceanic and Atmospheric Administration [NOAA, n.d.A] and Ocean Motion [NASA, n.d.B] section of the National Aeronautics and Space Administration (NASA). These organizations provide online real-time surface current databases freely available to the public on their web sites. Data related to the surface current is usually gathered using buoys, drifters and floats, high frequency radar and satellites. But surface currents are not the currents moving icebergs. Instead a near surface current, or shallow current, is the data needed for modelling [Turnbull et al., 2015].

The second major category of the current measurement technique is point natured methods and is mainly performed by tools called acoustic Doppler current profilers (ADCP) [Dinehart and Sacramento, 2003]. This method also has the drawback of not being able to provide the average magnitude across an area of interest. According to NASA's report on gathering methods [NASA, n.d.A], the main instrument for profiling the current in depths of several hundred of metres is still the ADCP, which is a single point current meter. NOAA also uses some deep water ocean drifters [NOAA, n.d.B] which go to 2,000 metres under water. Every 10 days, the drifters come to the surface in order to communicate wirelessly with the shore. The main disadvantage of these drifters is that they cannot provide real-time data. Furthermore, drifters can sometimes be lost or difficult to track especially in harsh sea conditions. Woods Hole Oceanography Institution [WHOI, n.d.] is

another organization that is actively involved in ocean related researches. It has moored profilers that provide an inventory of the current in a column of water using acoustic current meters. The recorded data is only downloadable when the instrument is recovered and again is not a real-time set of current information. Rossby [2016] has done a review on the use of ADCP and floats.

As the previous methods of ocean current measurement are not providing data at the desired depths, this paper proposes a technique for measuring the actual real-time value of the average current that can be deployed in a large section of the ocean. It consists of anchored acoustic sensor nodes along with stationary wireless devices for inter-node communications as well as communications with the shore station. With this setup, it would be possible to measure the shallow water current at any desired depth while avoiding the problems encountered with deep water drifters. A detailed explanation on the function of this setup and how much of the operations are performed under the water or in the air, as wireless signals, can be found in PRACTICAL COMPLICATIONS AND SOLUTIONS FOR IMPLEMENTATION.

As a small-scale prototype, the proposed method was tested at Memorial University's Fluids and Hydraulics Laboratory (FHL). The design of the experimental setup is presented in Attarsharghi and Masek [2014] which uses the transit time method [Lynnworth, 2013; Liptak, 2003] along with the cross correlation technique [Shin and Hammond, 2008]. This setup is appropriate for an accurate measurement of shallow water current. Based on this setup, a large-scale system could be deployed in open water. To the best of the author's knowledge and according to the recent researches and reviews on the ocean current measurement techniques [Pandian et al., 2010; Zuckerman and Anderson, 2014; Wilson et al., 2015], the complications of deploying such a system have never been addressed and reported in previous works.

As a result, this paper analyzes the achievements of the laboratory setup that were obtained from previous experiments, investigates deployment complications, and explains how the limitations in a lab-scale design were overcome. Techniques to make the laboratory outcomes applicable for the ocean environment are also proposed.

It should be mentioned that Dushaw et al. [2009] have also investigated the applications of acoustic signals in observing the ocean environment including ocean tomography. In ocean tomography, the average speed of sound is inferred from the time of flight and variations in the speed of sound are measured in order to calculate the changes in ocean temperature. A rule of thumb in this method is that a 1°C change in temperature corresponds to about a 4 m/s change in the sound speed [Munk et al., 2009]. Although this technique also uses the speed of sound for computations, it is different than the way the underwater sound speed was employed in the measurement discussed in this paper. In tomography, the two acoustic transducers are located very far from each other (100-500 km) and the speed of sound is considered to change over this distance. In this application, transducers are located relatively close to each other (about 3 km) as the wireless devices limit the distance among transceivers, so that the temperature and consequently the

speed of sound was considered to be steady and invariable in the target region. According to the ocean global data available in web sites such as NOAA [n.d.C], this is a confident assumption.

The rest of this paper is organized as follows. Basic theories of underwater sound propagation are explained in THEORY with specific investigation of transmission loss, noise, multipath and the Doppler effects and solutions to avoid their unwanted effects in the measurements. The research contributions are presented in PRACTICAL COMPLICATIONS AND SOLUTIONS FOR IMPLEMENTATION. First is the investigation of the practical aspects and limitations (e.g., electronic instrument limitations) faced in the lab-scale prototype and proposition of some solutions in order to make the design expandable and applicable in a large-scale area at desired regions in the sea. In this section, the optimal depth of the acoustic sensors in the target region of the ocean (which is offshore St. John's, NL, Canada, close to oil platforms) is proposed. Also, by means of Bellhop simulations [Porter, 2011] both eigenrays and transmission loss of the acoustic signals using actual hydrographic data are plotted. Thus, the effectiveness of the node placement scheme is proven with the simulation results. The Doppler effect, which is negligible in this case, is also discussed in the same section. Finally in CONCLUSION, research results and future steps are discussed.

THEORY

The underwater acoustic communication environment is different than the terrestrial environment with specific characteristics that should be taken into account while designing a network. Underwater acoustic channels are characterized by factors such as transmission loss, noise and multipath effect. Challenges with these phenomena were encountered in the lab-scale prototype and innovative solutions found, which is the basis of the proposal for a large-scale system. Their definitions along with related graphs are explained in the following sections.

Transmission Loss

Transmission loss or propagation loss (TL) is the loss in intensity in decibels (dB) and is described by the Urick [1983] propagation model in Equation (1) and depicted in Figure 1. TL is a function of the distance (d [m]) between the transceivers and the frequency (f [kHz]) of the acoustic waves. Medium absorption coefficient is shown by α (dB/km). The geometric spreading loss (χ) is of two types: spherical ($\chi = 20$), that characterizes omni-directional point source in deep water communications, and cylindrical ($\chi = 10$), which characterizes horizontal radiations in shallow water communications. The cylindrical χ is used in the calculations despite the fact that the transducers are omni-directional. Actually in theory, a point source of spreading energy means a source of spherical scattering, but it is not considered as such because, first of all, the area of the ocean where the systems is deployed, which is called Jeanne d'Arc Basin, around the oil platforms is considered as shallow depth (70-80 m) and is not an unbounded medium. Second, this medium is not a homogeneous medium, and the speed of sound varies between the channels because of the varying temperature and energy. Sound channels also trap energy. So the transducers tend to radiate energy like the surface of a cylinder within the channel of the water.

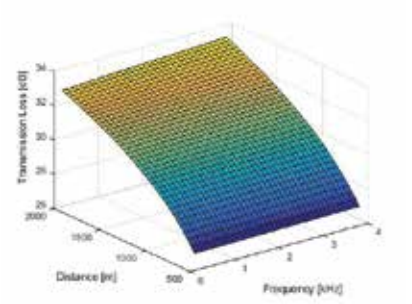

Figure 1: Transmission loss of intensity (dB) between transceivers located at various distances (m) from each other.

$$TL(d,f)= \chi.log(d)+\alpha(f).d\times 10^{-3} \quad (1)$$

Transmission loss increases with frequency and distance. These facts are used to design the large-scale current measurement system.

Noise

Noise is of two types: first, the ambient noise which is related to hydrodynamics like wind and rain, and second is manmade noise caused by shipping activities and machinery such as pumps [Stefanov and Stojanovic, 2011]. In the small-scale laboratory experiment (explained in the next section), a pump noise, caused by the machine used to run the water in a tank, was specifically experienced. This noise was successfully removed by proper filtering, which is discussed in Attarsharghi and Masek [2014]. A set of empirical formulae for the power spectral density (psd) of the noise was first defined in Coates [1989] and is expressed in the set of equations in Equation (2) in dB re µPa/Hz in which f is the frequency in kHz. Turbulence noise is N_t (dB re µPa/Hz) which is effective in frequencies lower than 10 Hz; N_s (dB re µPa/Hz) is shipping noise, with shipping activity $0 \leq s \leq 1$, for a range of frequencies between 10 Hz to 100 Hz; N_w (dB re µPa/Hz) is wind noise, with wind speed in m/s, which is effective in a wide range of frequencies 100 Hz-100 kHz; N_{th} (dB re µPa/Hz) is thermal noise for frequencies higher than 100 kHz; and w is the wind speed (m/s).

$$10logN_t(f)=17-30log(f)$$
$$10logN_s(f) = 40 + 20(s-50) + 26\log(f) - 60\log(f-0.03)$$
$$10logNw(f) = 50 + 7.5w^{0.5} + 20lof(f) - 40\log(f+0.4)$$
$$10logN_{th}(f) = -15 + 20\log(f) \quad (2)$$

Stojanovic [2007] sketched the psd for various wind speed and shipping activity and concluded that there exists a general linear approximation in logarithmic scale to substitute all these four components. The generic linear format that is sketched by the same author can be formulated here by Equation (3) and is sketched in Figure 2. This approximation is used in the calculations for a large-scale design of the current measurement system.

$$10logN(f) = 95 - 15*log(f) \quad (3)$$

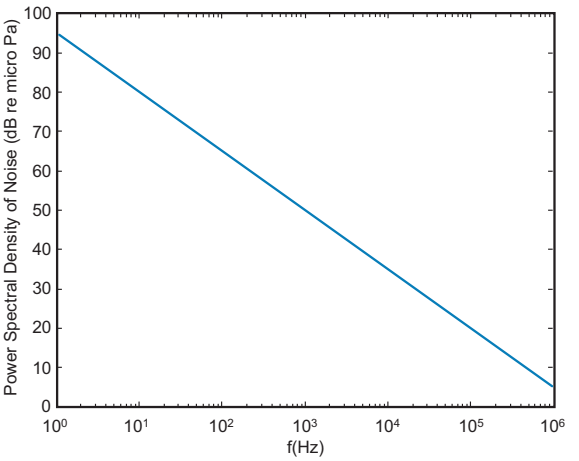

Figure 2: Demonstration of the approximation of ambient noise power spectral density (dBre µPa/Hz).

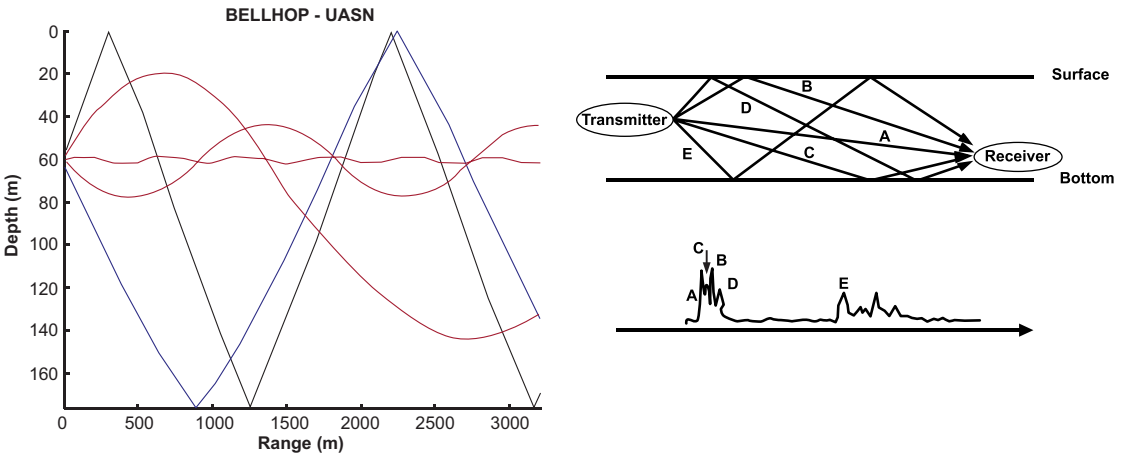

Figure 3: Multipath effect. Left: Eigenrays sketched in Bellhop using hydrographic data for the ocean condition from Fisheries and Oceans Canada [2015]. Right: Schematic diagram of the multipath phenomenon; A to E are different paths. Right bottom: Multipath intensity profile of the rays travelling through the A to E paths [Lurton, 2002].

Multipath

Multipath is formed because of the sound ray reflections from the surface and bottom and also because of refractions, which are due to the sound speed variability that is a result of changing temperature, salinity and pressure with depth and location. For the sound refractions, rays tend to bend toward the region in water where the sound speed is lower according to Snell's law [Jensen et al., 2011]. In Figure 3, eigenrays, which are red, manifest the refraction effect and the other two colours are showing the reflection effect.

Figure 4 shows that the speed of sound increases with the increase in temperature and pressure.

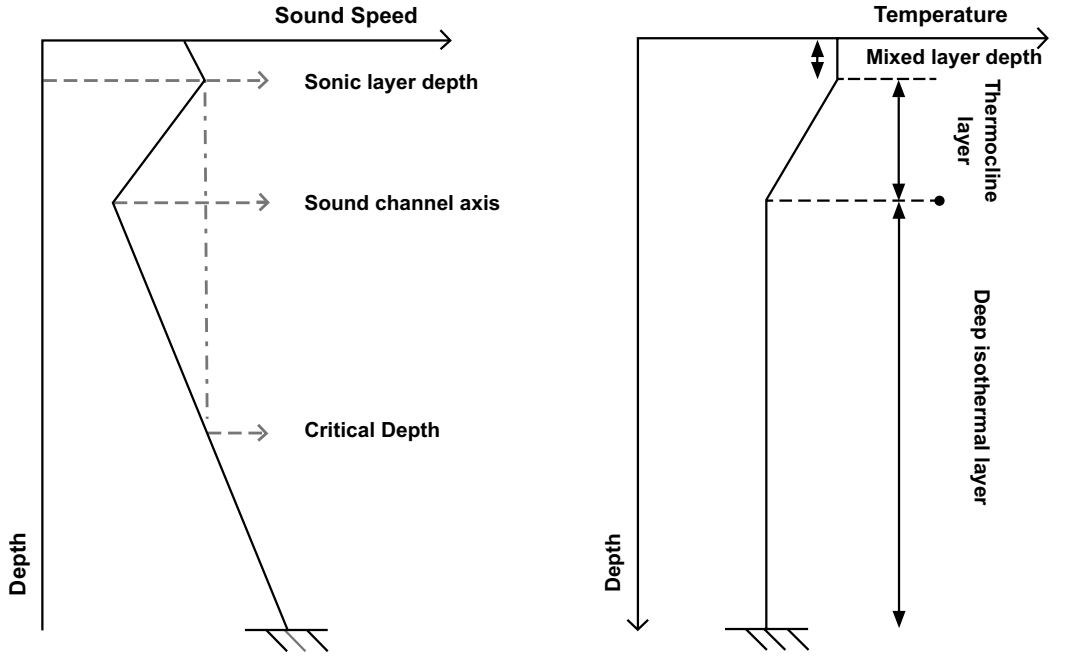

Figure 4: Left: Sound speed profile schematic. Right: Temperature vs. depth in the ocean.

In the thermocline zone, temperature decrease is the reason of the decrease in the sound speed [Etter, 2013] but deeper in the isothermal zone, the pressure is the main factor in the sound speed increase.

According to Jensen et al. [2011] and Stefanov and Stojanovic [2011], an intensity loss is associated with the sound ray reflections (about 3 dB from the bottom). So, if the rays could travel a straight path, they face less intensity loss and arrive sooner at the receiver. This fact along with the whole concept of multipath effect is being used throughout this paper and a solution is shown to eliminate this unwanted effect in the experimental results using the sample window technique. The technique proposed for the large-scale system deployment and an optimal depth positioning idea are described in PRACTICAL COMPLICATIONS AND SOLUTIONS FOR IMPLEMENTATION.

Doppler Shift

Transmitters and receivers move with the waves and the flow of the current. If v_s is the speed of the transmitters' movement in m/s and v_r is the receivers', then the Doppler shift phenomena causes a change between the emitted frequency (f_0 in [Hz]) and the observed frequency (f in [Hz]), which is associated to these movements [Gill, 1965] and is expressed by Equation (4). In Equation (4), c (m/s) indicates the speed of sound in water. The Doppler shift could actually affect and intervene in high rate data transfers in acoustic communications. But as proven in the next section, and as the acoustic transactions in this case are not considered as a high rate communication in the current measurement system, this shift is considered to be very small and can be totally neglected in the current monitoring process.

$$f = \frac{c + v_r}{c + v_s} f_0 \tag{4}$$

PRACTICAL COMPLICATIONS AND SOLUTIONS FOR IMPLEMENTATION

A lab-scale prototype of a current measurement system has been designed and implemented, with the schematic sketched in Figure 5, based on the transit time method and cross correlation technique along with synchronization of two acoustic nodes. According to the schematic diagram, the synchronization phase is performed wirelessly outside the water. The modules which are involved in the synchronization phase are GPS (synchronization unit in Figure 5) and ZigBee units (wireless communication module in Figure 5). The underwater communication

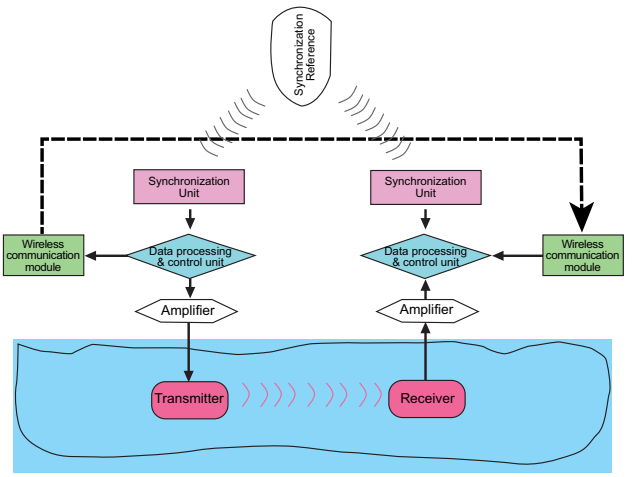

Figure 5: Current measurement system block diagram. The wireless modules are Zigbee wireless unit, GPS is the synchronization unit. Calculations and algorithms are implemented and performed with the Arduino microprocessor.

units, which consist of the transceiver and their drivers that are connected to the wireless modules, receive the commands from the wireless devices and perform the acoustic communications. More details about the process are explained later in the descriptions related to Figure 6. The lab-scale experiment has been performed in a tank with adjustable flow rate at Memorial University's FHL and the details of the results are published in Attarsharghi and Masek [2014]. This experiment is a basic block of an expanded system for a larger scale implementation. Communication between two acoustic nodes and the designed driver and amplifier for the transducers have been successfully tested.

An overview of the logic behind this process is explained in the state machine diagram of Figure 6 (top) in which a design of a system

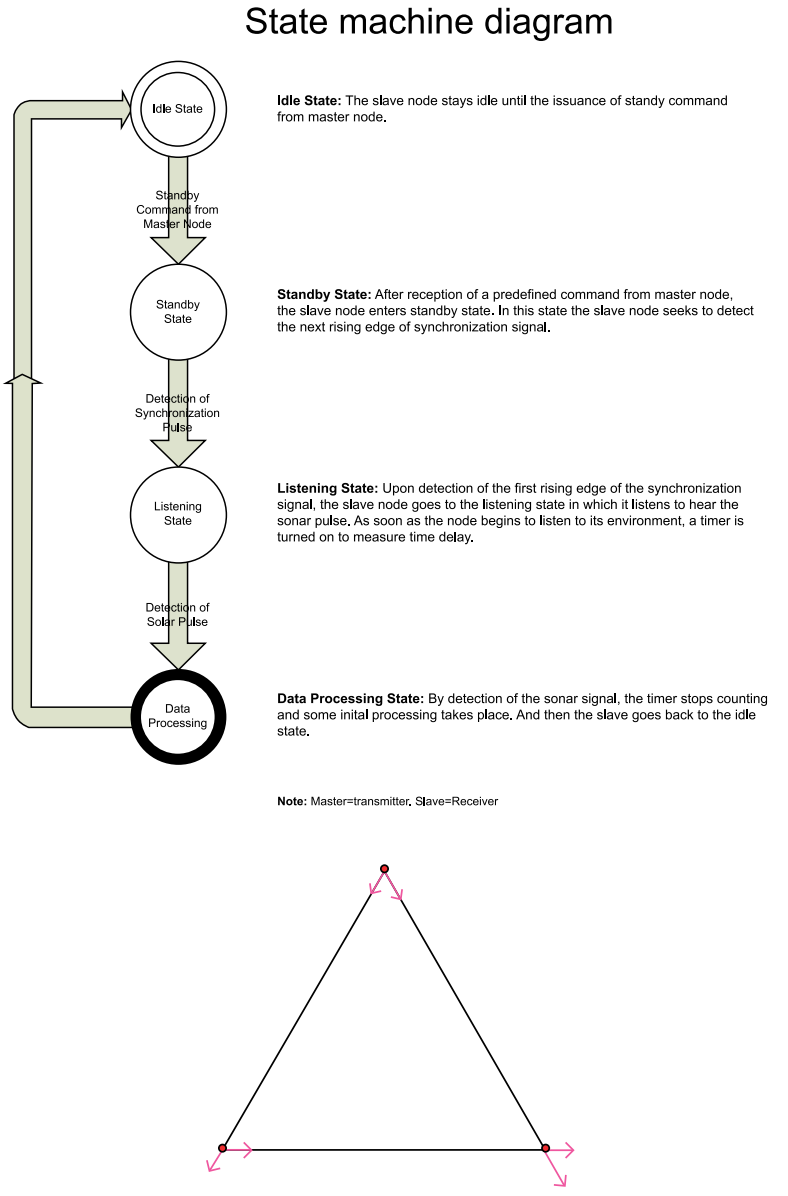

Figure 6: Top: State machine diagram at the receiver. Bottom: Basic triangular cell for measuring the current vector.

that could be implemented in the shallow water at the target area, which is where oil platforms are located at Jeanne d'Arc Basin in the North Atlantic Ocean, is proposed. The wireless Zigbee module at the transmitter side sends wireless signals to the receiver to alert it to be ready for the reception of the acoustic signals. After sending this message, the transmitter projects the acoustic pings into the water at the rising edge of the pulse-per-second (PPS) output of the GPS device (synchronization unit). The receiver, which is in standby mode, records the received acoustic signal, once the PPS signal arrives and the microprocessors at the receiver perform signal processing computations. More details on the signal processing of the received acoustic waves can be found in Attarsharghi and Masek [2014].

The triangle at the bottom of Figure 6 demonstrates the basic block of the acoustic network. Acoustic nodes form triangular cells in order to measure the average vector of the shallow water current. In Figure 6 top, according to the process described in the state machine diagram employing transit time method, the vector of current is measured between each two nodes, and the summation of two vectors on each node gives the final current vector at each vertex. This process gives the map of the current in the desired zone. The setup details, including drivers' and amplifiers' design, and the result of calculations in the microprocessor are explained in Attarsharghi and Masek [2014].

Now according to the fact that the prototype is functional, in the following sections, the actual situation and environment, in which the whole network is supposed to be implemented, is investigated. Practical concerns and solutions that are important factors affecting the functionality of the system in the ocean are also mentioned.

Precision in Analysis

In this section, according to the experimental practice in the lab-scale prototype, a delicate practical strategy related to the time-delay measurement using the cross correlation technique along with transit time method is explained. Details of the technique along with experimental results are described in Attarsharghi and Masek [2014].

Precision analysis was performed in order to avoid inaccuracies and errors in the process of time measurement. In the transit time method used in the lab, which is also the basis of the current measurement process in the proposed system for the ocean, accurate measurement of the time is crucial. Here is a concise description of the complete process introduced in Figure 6. In Figure 7, PPS signal of the GPS device is depicted. The transmitter sends the acoustic signal with the rising edge of the PPS pulse at t_1, and the data received from the A/D port of the microprocessor at the receiver is stored in the receiver's memory. The received signal is cross correlated with the main emitted signal that has already been stored in the memory of the receiver, resulting in a signal with a peak around its midpoint. This peak is a sign of the complete receipt of the transmitted signal. The travel time or time-delay is therefore the difference between the time at which this peak occurs and the moment of the rising

edge of the PPS that the transmitter initiates sending acoustic signals. The important practical point is that the value of $\frac{pulsewidth}{2}$ should be deducted from this measured time as the actual time-delay is equal to t_2-t_1 in Figure 7. This is due to the fact that t_1 is the point of the initiation of the rising edge of the pulse (depicted in Figure 7) and the microprocessor at the receiver should flag an end of the time when the front edge of the acoustic signals are sensed. In practice, this stop point is considered to be at the time when the cross-correlated signal's peak happens. This is a constant offset that should not be counted in the measurement of t_2-t_1. In other words, as Figure 7 shows, if this amount is not deducted from the result, because the peak appears somewhere after t_2, this causes an error in the time calculation. This is an important point that should be observed in developing the measurement algorithm in the large-scale system as well.

Multipath Effect

In the previous section it was mentioned how multipath propagation occurs. In order to avoid the interference of the signals that the multipath effect causes as well the inaccuracy and error of the measurements mentioned in Attarsharghi and Masek [2013A], the best depth of acoustic sensors deployment is proposed in the following section, which is especially useful in the ocean. The multipath effect in the lab was practiced and overcome with a similar technique which was a proper design of the transceivers' distance from each other, from the walls of the tank as well as from the surface of the water [Attarsharghi and Masek, 2014].

Best Depth for Deploying the System in Large-Scale along with MatLab/Bellhop Simulation Results

In this section, the best depth for transducers to be deployed is obtained and, by using Bellhop, (a MatLab toolbox that deterministically

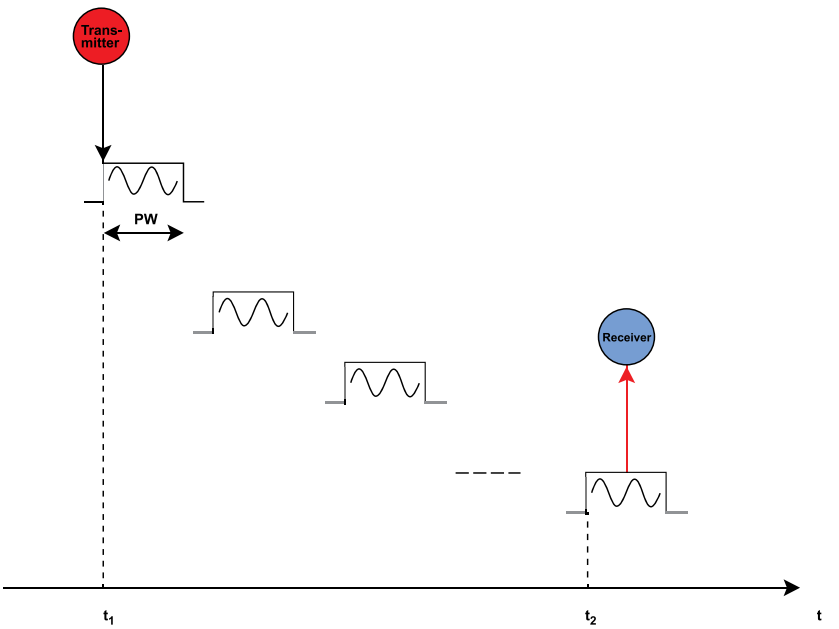

Figure 7: Timing diagram of the pulse-per-second pulse of the GPS device at the transmitter and receiver. PW stands for the pulse width. The red arrow is the time when the cross correlation's peak happens.

describes underwater acoustic channels [King et al., 2010]), a real case scenario in the Northwest Atlantic Ocean, Jeanne d'Arc Basin region, is simulated to prove the effectiveness of this new idea. Furthermore, it is demonstrated how this optimal depth contributes to less measurement error as well as less energy consumption.

For the large-scale system simulations, hydrographic data for the calculations in the above mentioned area were extracted from the Canadian Government web site [Fisheries and Oceans Canada, 2015] available at Oceanography and Scientific Data, Atlantic Zone Monitoring section. Below are the details on the location.

Hydrographic Data: Data view
Station: Station 27
Location: 47.55ºN 52.59ºW
Year: 2015

Using the above dataset for temperature (T [°C]), salinity (S [psu]) and depth (Z [m]), sound speed profiles (SSPs) were calculated using Equation (5) [Etter, 2013] and the graphs sketched in MatLab (Figure 8). In the equation below, C is the speed of sound in the water (m/s).

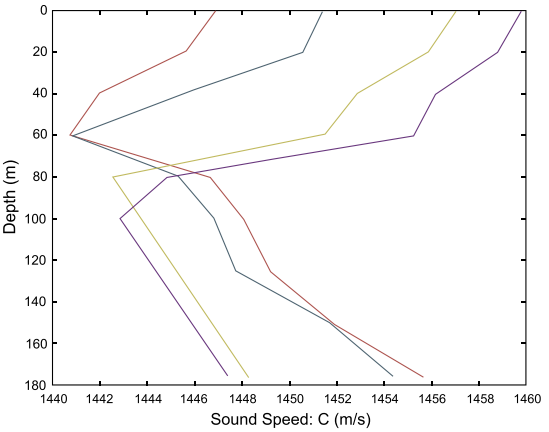

Figure 8: Sound speed profile in different seasons in the North Atlantic Ocean.

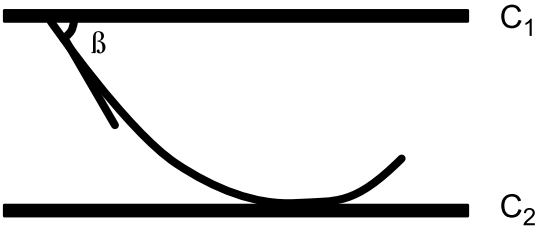

Figure 9: Propagation of sound along an arc of a circle.

$$C = 1449.2 + 4.6\times T - 0.055\times T^2 + 0.00029\times T^3 + (1.34\text{-}0.010\times T) \times (S\text{-}35) + 0.06\times Z \quad (5)$$

The SSP graphs define a sound channel, as was mentioned earlier in Figure 4. The SSP curves are segmented into short linear sections representing the sequence of layering. Inside the layers, sound changes slightly with a constant rate.

Propagation of sound in such layers is along an arc of a circle (Figure 9) and it bends towards the side of the lower speed until entering into the next layer and travelling along another circle arc with different curvature again. The size of the radii of the circles depends on the rate of the sound speed change: the slower it changes, the larger the radius. Sound ray path is composed of connecting sections of the circles. Therefore, the depth in which the sound speed profile is minimum, that is the channel axis in Figure 4, is located on the layer with constant sound speed where the change is almost zero. In this layer, circles have a very large radii, which means straight propagation of rays (waveguide) with the least reflection or refraction loss [Wille, 2005]. The increase in sound speed above the channel axis is due to the temperature and below is due to pressure [Brekhovskikh

and Lysanov, 2003]. Below is the rationale behind this theory.

The curvature is defined in relation to the grazing angle loss [Wille, 2005] (between the ray and the constant depth plane) in Equation (6):

$$g_n = \frac{c_n - c_{n-1}}{z - z_{n-1}} \quad , R_{cn} = \frac{c_{n-1}}{g_n \cos\beta_{n-1}} \tag{6}$$

Where R is the radius of the curvature (m), g is the velocity gradient (1/s), ß is the grazing angle, c is the velocity of the sound in water (m/s), z is depth (m) and n is the index associated to the layer. Therefore, when the gradient of c is close to zero, the radius is very large.

In the next section, different depth of sources (using the specification of Aquatrans [DSPcomm, 2009] transducers) in different seasons (various SSPs) with the environmental conditions at the target area of interest are simulated (Figures 10 and 11). As can be seen, if the source is placed in the channel axis with the least sound speed, c_{min}, signals arrive faster without undergoing any curvature.

Therefore, for capturing the acoustic rays at the receiver, a sampling-time-window can be defined accordingly which has a width proportional to c_{min} in order to minimize the error caused by multipath propagation. Details

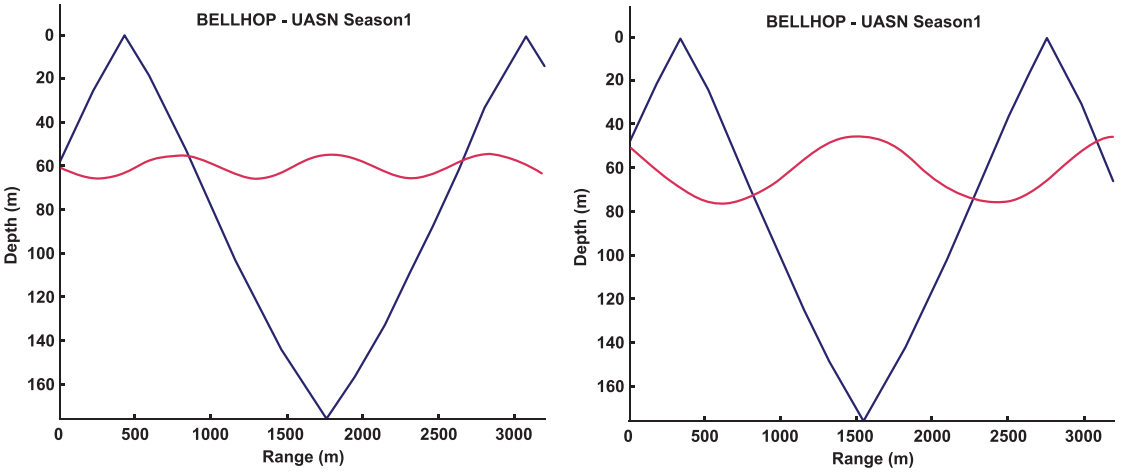

Figure 10: Season 1 – Best depth (d) 60 m. Left: f=7500 Hz, d=60 m. Right: f=7500 Hz, d=50 m.

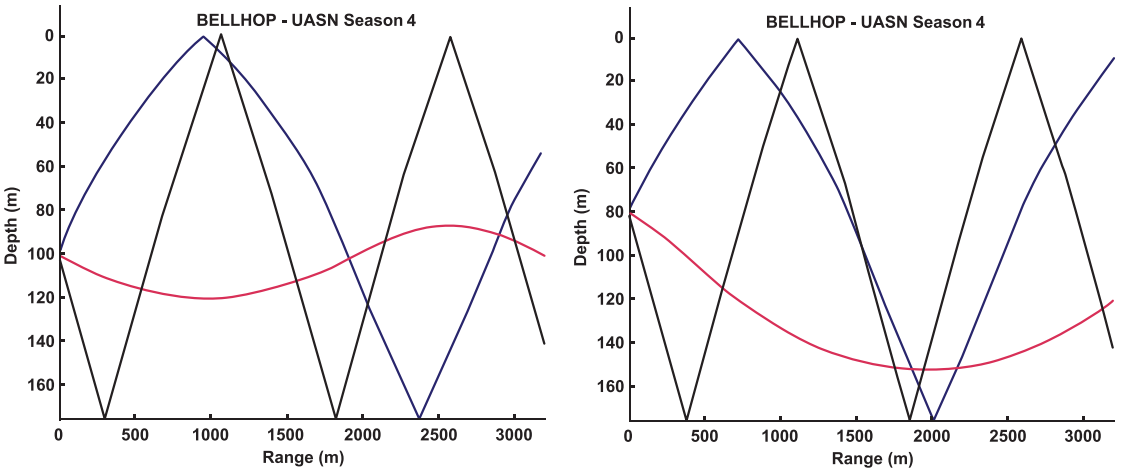

Figure 11: Season 4 – Best depth 100 m. Left: f=7500 Hz, d=100 m. Right: f=7500 Hz, d=80 m.

about how to calculate the width of this window and when to activate it is described in Attarsharghi and Masek [2014] and was practically proven to be efficient by proper positioning of the transducers during prototype testing. Therefore, the receiver does not capture eigenrays coming after the straight fast rays. So with this optimum depth deployment, the straight path is the only one captured and others are eliminated using this windowing technique, and acoustic signals that reach the receiver face less energy loss due to the fact that there are no reflections or refractions. This means the amount of power required to be consumed in the transmitter part is less than the condition in which there is multipath effect which will result in energy savings. Providing energy is a huge concern in large-scale ocean deployments.

Eigenray Plots

Figures 10 and 11 are simulation results with Bellhop, depicting different depths of transceivers and different SSPs at different seasons. Physical parameters like depth, temperature and salinity result into various speeds of sound in different seasons. Therefore, the performance of the transducers in various underwater conditions is evaluated.

As can be seen, the best depth only depends on the channel axis which is obtainable from SSP. When the transceivers are located in other depths it takes longer for the eigenrays to travel the same path as the multipath affects the rays' routes. Therefore the whole measurement system deflects from its optimal functionality. This idea could be applicable in large-scale as well. Details are explained in the following section.

Suggestion for Further Improvement

As depicted in Figure 8, best depth depends on the water condition (temperature, salinity, etc.) which is a variable parameter. Therefore, in order to always maintain the optimum depth, the nodes should be able to move along an anchor in a fixed column. A propeller which is installed along with the acoustic transducers could handle the vertical movement of the node. The node's microprocessor could control the movements according to the water condition and the related SSP. Therefore the system could be deployed in the ocean for the current measurement application.

In the next sections, after selecting a proper communication range, the transmission loss of the acoustic signals are plotted for AquaTrans transducers used in the lab; the optimum path is also observable in these plots. The reason that lab equipment is used as examples is to show that the setup is expandable in a large section of the ocean.

Sensitivity and Transmission Loss Calculations

Now the intensity loss that acoustic signals face while travelling a certain distance under the water are calculated; various conditions are simulated; and the resultant transmission losses are plotted. For the distance that acoustic rays travel, a reference inter-node distance must be set: 3.2 km was chosen as this distance is the range of the wireless modules that were used in the prototype. This range imposes a limit to the node communications. The ZigBee wireless modules' specifications can be found in the device's datasheet [Parallax, n.d.]. In the following, it is shown how the lab setup, under the proposed new conditions, could be

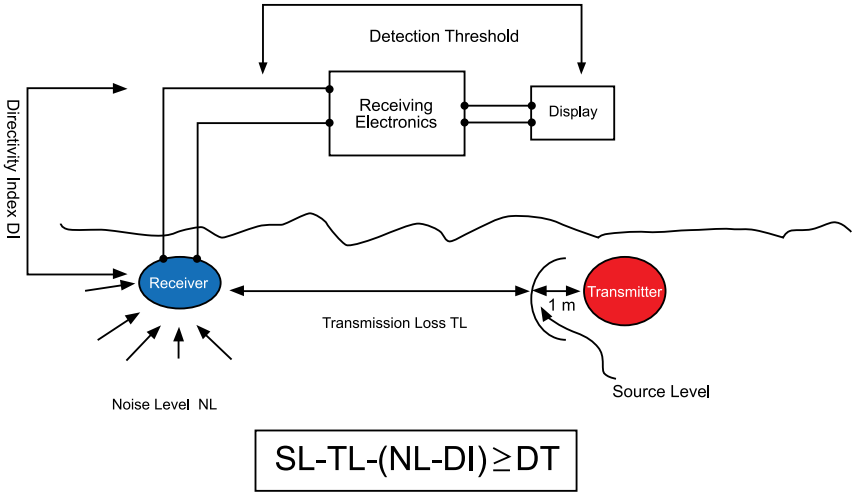

Figure 12: Passive sonar equation diagram. SL is the source level, NL is the noise level, DI is directivity index of the transducer, which is zero for omni-directional transducers (in the lab-scale experiment), and DT is the detection threshold [Lurton, 2002].

implemented in the target zone in the ocean and the eigenrays emitted from the source node can reach the set inter-node distance to be processed and give an accurate in-situ real-time measurement of the current. In order to continue, Figure 12, which is a schematic diagram of the passive sonar equation, depicts how each sentence in the equation can be calculated [Lurton, 2002].

Start with the detection threshold in Figure 12. For the receiving electronics, the Arduino-Uno [2016] modules were used in the lab as the interface board. These modules have a built-in microprocessor [Atmel, 2016] with 8 bit A/D converter (ATmega328P 2016). This means in order to have a detectable voltage at the receiver, a minimum voltage of 0.02 V is required. Therefore, other parameters such as distance and transmitted voltage intensity need to be set so that the voltage that reaches the receiver is strong enough to be detected. Having the distance and the intensity of the transmitter set to 350 volts peak to peak [Attarsharghi and Masek, 2013B], the conditions for the large-scale deployment are investigated.

For investigating the signal intensity at the hydrophone or the receiver, the electrical circuitry needs to be investigated. In the lab-scale experiments a low noise amplifier, LM1875, was used at the receiver, which is specifically designed for acoustic applications. It was designed to have a gain of 20 which could be cascaded to another similar amplifier, though only the first stage was used in Attarsharghi and Masek [2013B] as the intensity of signal was high enough in the lab. However, as it is mentioned in Attarsharghi and Masek [2013B], the other stage is specifically implemented for very weak signals that is useful in the large-scale conditions and will result in a gain of 400. There is also a band pass filter with a gain of almost 1 with 3 dB ripple. This gain could be designed to further boost the gain if necessary in its pass band. So the overall gain ($G_{overall}$) of the electrical circuit at the receiver which is the product of the gain of the low noise amplifier (G_{LNA}) and the gain

of the filter (G_{filter}) [Attarsharghi and Masek, 2013B] is defined by Equation (7) as:

$$G_{overall} = G_{LNA} \times G_{filter} = 400 \quad (7)$$

As the resolution voltage (or the minimum detectable voltage) is 0.02 V, at the analog to digital converter input pin of the microprocessor, this translates to a voltage of $0.02/400=5 \times 10^{-5}$ at the receiver output. Therefore the threshold voltage at the receiver (dB) is given by Equation (8).

$$VdB_{threshold@receiver} = 20 \times \log(5 \times 10^{-5}) = -86.02\ dB \quad (8)$$

According to Figure 12 the passive sonar Equation (9) is:

$$SIL_{receiver} = SL - TL - (NL - DI) \geq DT \text{ (or } VdB_{(threshold@receiver)}) \quad (9)$$

Where $SIL_{receiver}$ is signal intensity level at the receiver (dB) and DT is the detection threshold (dB) which is equivalent to $VdB_{threshold@receiver}$.

Also below is the sonar Equation (10) at the receiver (dB):

$$VdB_{receiver} = SIL_{receiver} + OCRR \quad (10)$$

The open circuit voltage response of the receiver (OCRR or OCVR) (dB re 1V/µPa) is a specification of the ultrasonic transducers (refer to APPENDIX for AquaTrans OCRR specifications). Therefore, for the above equation to be true, $SIL_{receiver}$ should be properly achieved.

As mentioned, the amplified voltage at the transmitter in the lab-scale experiment could easily reach $350V_{pk-pk}$ which is equal to $124\ V_{rms}$. So the transmitting voltage in dB is defined in Equation (11).

$$VdB_{transmitter} = 20 \times \log(124) = 41.86\ dB \quad (11)$$

And according to the specification sheet of AquaTrans (see APPENDIX), transducers have a transmitting voltage response (TVR) of 132 dB at around 7500 kHz.

At the transmitter there is the following sonar Equation (12):

$$SIL_{transmitter} = TVR + VdB_{transmitter} \quad (12)$$

Where $SIL_{transmitter}$ is the sound intensity level at the transmitter. This means that the sound intensity at the transmitter is 173.86 dB according to Equation (13).

$$SIL_{transmitter} = 132 + 41.86 = 173.86\ dB \quad (13)$$

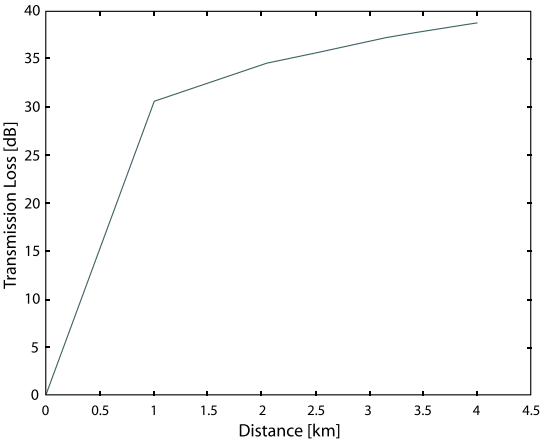

Figure 13: Transmission loss vs. distance at 7.5 kHz.

This is the sound level which reaches the receiver at 3.2 km (which is dictated by the

limitation of the ZigBee module wireless device) distance of the transmitter.

The performance of the transceivers at 7.5 kHz at which OCRR $_{7.5kHz}$ = -190, NL = 32.5 dB (Figure 2) is investigated. By having the TL Equation (2) for cylindrical propagation of sound, Figure 13 gives $TL_{3.2\ km,7.5kHz}$ = 37.3 dB which from Equation (9) leads to sound intensity level of 103 dB according to Equation (14).

$$SIL_{receiver} = 173.86\text{-}37.3 - 32.5 = 103\ dB \qquad (14)$$

So from Equation (10) the receiver voltage in dB can be calculated by Equation (15):

$$VdB_{receiver} = SIL_{receiver} + OCRR = 103 - 190 = -86\ dB \qquad (15)$$

As can be seen $VdB_{receiver}$ is equal to the detectable threshold (-86.02 dB). So this system with the current circuitry design is suitable to be implemented in the open water in large-scale with a node distance of 3.2 km at 7.5 kHz of frequency, if the proposed optimal depth is observed so that signals do not suffer any extra intensity loss. To be able to avoid the inaccuracy and reduce error in the calculations caused by multipath interference of the signals, the right sampling window time needs to be defined similar to the method practiced in the lab.

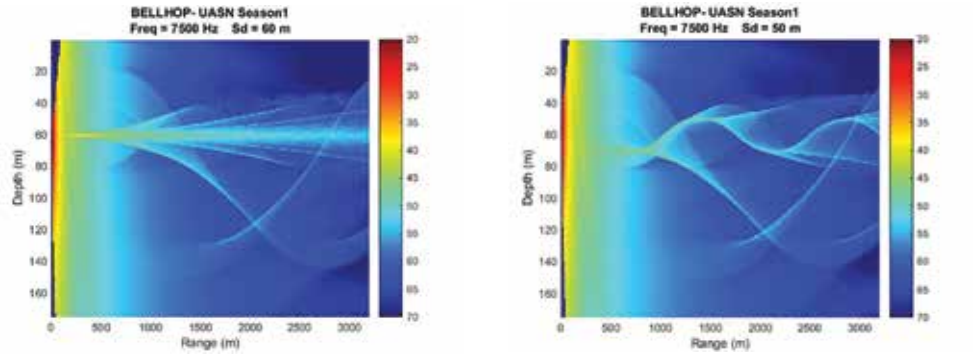

Figure 14A: Season 1 – Transmission loss with source or transmitter (sd) in different depths. Left: At optimum depth. Right: At a non-optimum depth.

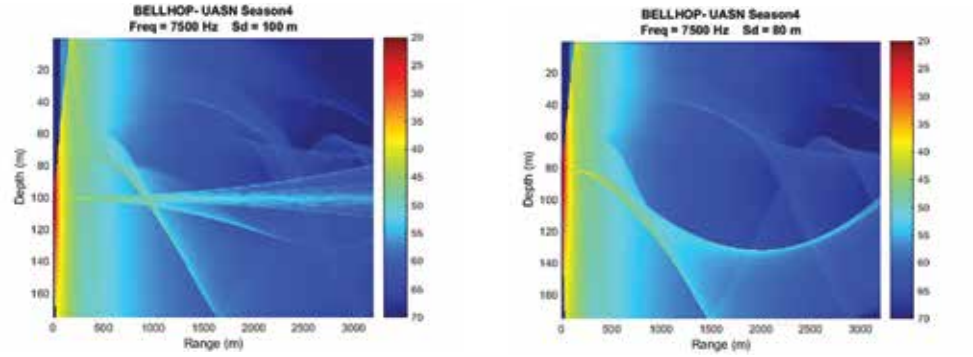

Figure 14B: Season 4 – Transmission loss with source or transmitter (sd) in different depths. Left figure shows that if the source is located at the proposed optimum depth, intensity loss is in a range (40 dB in this case) so that the detection threshold criteria at the receiver could be met. In the right figure it is obvious that the waves lose more intensity and take more time to reach the receiver which causes interference for the signal processing phase.

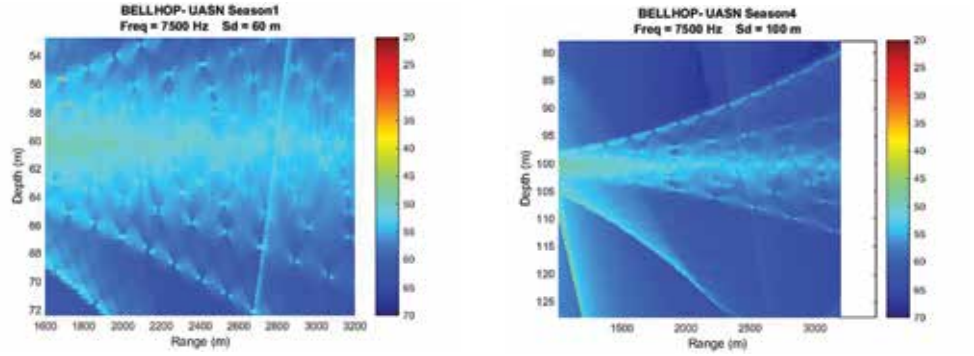

Figure 14C: Zooming into the signal intensity at the receiver (located at 3.2 km in this case) showing the intensity loss in optimum depth case for the two different seasons is appropriate to be detected (40 dB loss).

Simulation results in the next section also confirm that the intensity of the sound waves at the receiver meets the sensitivity criteria of the AquaTrans hydrophones in the set inter-node distance in the ocean.

Transmission Loss Plots

According to the simulated environment in MatLab/Bellhop with actual hydrographic data and the previous section numerical analysis, in Figure 14 (A and B) TL plots are confirming the calculation results in the section above (intensity loss is about 40 dB which in the similar level of the calculation results is 37.3 dB). This is an additional remark of the effectiveness of the proposed ideas that shows the lab-scale design is deployable in the open water at the target region: Jeanne d'Arc Basin. In Figure 14A (left) transmission loss is depicted in season 1 water condition with the source located at the proposed optimum depth. Intensity loss is small enough (40 dB in this case) so that the detection threshold criteria at the receiver could be met. In Figure 14A (right; non-optimum depth) it is obvious that the waves lose more intensity and take more time to reach the receiver which causes interference for the signal processing phase. In Figure 14B the same scenario has been simulated but in season 4 which has a different water condition. Figures 14A and 14B show similar results for the optimum and non-optimum transceiver depths. Figure 14C shows the focused picture of the signal intensity at the receiver in the optimum depths condition in season 1 (Figure 14C, left) and season 4 (Figure 14C, right).

As can be seen in Figure 14, the best depth in each season is observable and, if the source depth is set at that optimum depth, signals at the receiver will be easier to detect without experiencing a severe multipath effect in the large-scale design.

The next section investigates how it is possible to neglect the Doppler effect in the large-scale measurements design.

Doppler Effect

Previously, it was mentioned that the Doppler shift is one of the concerns in propagation of the sound rays. Here it is explained how this interference could be avoided in the ocean current measurement process. First the equations related to the Doppler effect (Equations (16) and (17)) are defined. In these equations, f is the observed frequency (Hz) and

f_0 is the transmitted one (Hz), c is the speed of sound under the water (m/s), $\Delta v = v_r - v_s$ is the difference between the speed of the transmitters' movement and the receivers' (m/s) and the Doppler effect is Δf (Hz).

$$f = (1 + \frac{\Delta v}{c}) f_0 \quad (16)$$

$$\Delta f = \frac{\Delta v}{c} f_0 \quad (17)$$

As can be seen, the Doppler effect or Δf is proportional to c^{-1} that is roughly 1500^{-1} which is equal to 6.6667×10^{-4}. According to the real-time data downloaded from Ocean Surface Current Analyses Real-Time web site [NOAA, n.d.C], surface current speed is in the order of 1 m/s. So Δv is very small in comparison with c^{-1} and consequently the Doppler effect is very small and negligible. In order to compute the maximum frequency deflection, v_r and v_s could be considered in exactly opposite directions. In other words, transducers could be considered to move with current with the speed of $v_r = 1$ and $v_s = -1$. These values for the speed of current result in $\Delta f_{max} = 4Hz$. As mentioned above, this is a very small deflection and does not affect the computations. It is also very small compared to the band-pass filter's band width at the receiver in Attarsharghi and Masek [2013B] so that does not interfere with the signal's receiving process at the receiver. Actually, the Doppler effect in higher frequencies (40 K-3000 KHz) is big enough to be useful in instrumentation like ADCPs.

CONCLUSION

The presented work first examined the underwater acoustic wave propagation in terms of losses, noise, multipath and the Doppler effects. Then practical techniques for the deployment of a networked system for ocean current measurement were proposed and elaborated. These techniques have been implemented in the lab-scale experimental setup making it ready for a large-scale system deployment. The precision analysis in calculating the time delay provides a practical strategy to reduce the measurement error. Also, an ideal depth placement is proposed, based on theoretical analysis, which leads to a new technique aimed to make the lab-scale verified system feasible in open water, with the least measurement error possible. Software simulation results were provided, using actual real-time hydrographic data, in order to support the theoretical ideas and expand the lab results to an ocean-scale design of measurement system.

Currently, research on an underwater sensor network for ocean current monitoring is being conducted using the rules developed in this work. While the depth placement was discussed here, the combination and the lateral placements of acoustic nodes, aiming for an energy efficient topology, will be considered in future research.

APPENDIX

Below are the transmitting voltage response (TVR) and open circuit voltage response (OCR) of the AquaTrans acoustic transducers used in past lab experiments.

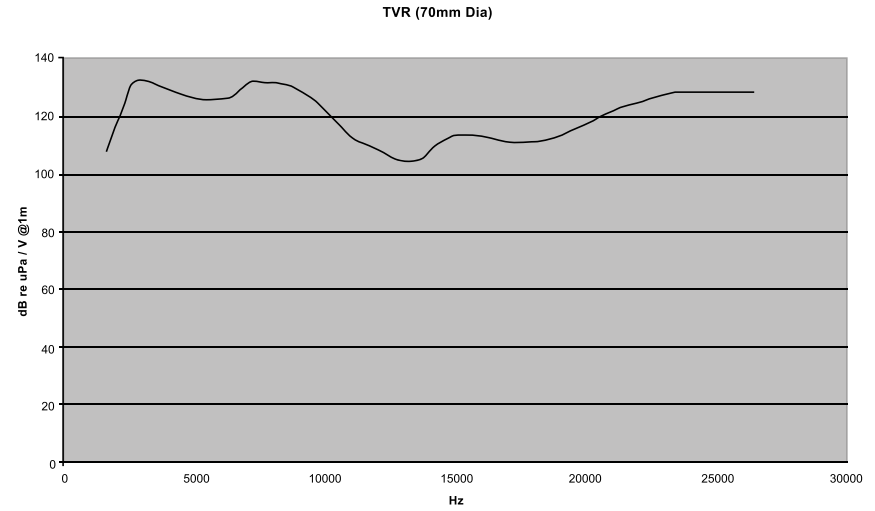

AquaTrans transmitting voltage response (TVR); from producer's technical catalogue.

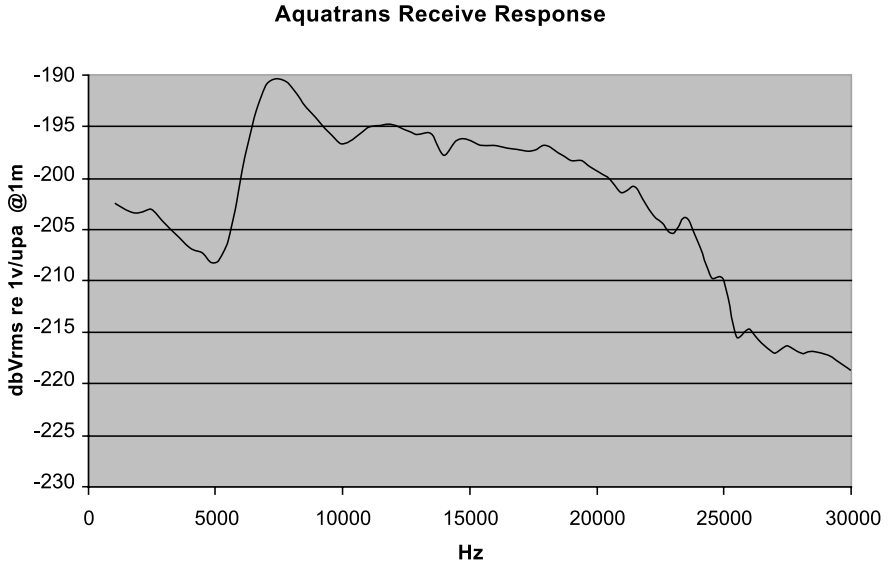

AquaTrans open circuit voltage (OCV) response at the receiver; from producer's technical catalogue.

REFERENCES

Arduino-Uno [2016]. *Uno microcontroller board overview*. Retrieved from: www.arduino.cc/en/Main/ArduinoBoardUno.

Atmel [2016]. *8-bit Atmel microcontroller, ATmega328P*. Retrieved from: www.atmel.com/devices/atmega328.aspx.

Attarsharghi, S. and Masek, V. [2013A]. *Modeling underwater multiple path effect on the measurement of water velocity.* NL Electrical and Computer Engineering Conference (NECEC'2013), St. John's, NL, Canada. Retrieved from: http://necec.engr.mun.ca/ocs2013/viewabstract.php?id=31.

Attarsharghi, S. and Masek, V. [2013B]. *Underwater acoustic driver/amplifier design and implementation*. NL Electrical and Computer Engineering Conference (NECEC'2013), St. John's, NL, Canada. Retrieved from: http://necec.engr.mun.ca/ocs2013/viewabstract.php?id=32.

Attarsharghi, S. and Masek, V. [2014]. *Ocean current monitoring via cross-correlation technique and node synchronisation*. IEEE Oceans, St. John's, NL, Canada. Retrieved from: http://ieeexplore.ieee.org/xpls/abs_all.jsp?arnumber=7003049&tag=1.

Brekhovskikh, L.M. and Lysanov, Yu.P. [2003]. *Fundamentals of ocean acoustics, 3rd edition*. Springer Science and Business Media, ISBN 978-0-387-95467-7.

Chapman, P.; Wills, D.; Brookes, G.; and Stevens, P. [1999]. *Visualizing underwater environments using multifrequency sonar*. IEEE Computer Graphics and Applications, Vol. 19, Iss. 5, pp. 61-65.

Coates, R.F. [1989]. *Underwater acoustics systems*. Halsted Press, John Wiley and Sons Canada. ISBN 0470215445, 9780470215449.

Dinehart, R.L. and Sacramento, C. [2003]. *Spatial analysis of ADCP data in streams*. Proceedings, Federal Interagency Sediment Monitoring Instrument and Analysis Research Workshop. Retrieved from: http://water.usgs.gov/osw/techniques/sediment/sedsurrogate2003workshop/dinehart.pdf.

DSPcomm [2009]. *AquaTrans – underwater acoustic dunking hydrophone transducer*. Retrieved from: www.dspcomm.com/products_aquatrans.html.

Dushaw, B.; Au, W.; Beszcynska-Moller, A.; Brainard, R.; Cornuelle, B.; Duda, T.; Dzieciuch, M.; Forbers, A.; Freitag, L.; Gascard, J.-C.; Gavrilov, A.; Gould, J.; Howe, B.; Jayne, S.; Johannessen, O.; Lynch, J.; Martin, D.; Menemenlis, D.; Mikhalevsky, P.; Miller, J.; Moore, S.; Munk, W.; Nystuen, J.; Odom, R.; Orcutt, J.; Rossby, T.; Sagen, H.; Sandven, S.; Simmen, J.; Skarsoulis, E.; Southall, B.; Stafford, K.; Stephen, R.; Vigness-Raposa, K.; Vinogradov, S.; Wong, K.; Worchester, P.; and Wunsch, C. [2009]. *A global ocean acoustic observing network*. Proceedings, OceanObs'2009, Vol. 2. Venice, Italy. 10.5270/OceanObs09.cwp.25.

Eik, K. [2009]. *Iceberg drift modelling and validation of applied metocean hindcast data*. Cold Regions Science and Technology, Vol. 57, No. 2, pp. 67-90.

Etter, P.C. [2013]. *Underwater acoustic modeling and simulation*. CRC Press. ISBN 9781466564930.

Fisheries and Oceans Canada [2015]. *Hydrographic data: data view*. Retrieved from: www.meds-sdmm.dfo-mpo.gc.ca/isdm-gdsi/azmp-pmza/hydro/station/graph-eng.html?a=0&v=PSAL&k=c&y=2015.

Gill, T.P. [1965]. *The Doppler effect: an introduction to the theory of the effect*. Logos Press, London. ISBN 10: 1124112979; ISBN 13: 9781124112978.

Gough, P. and Hawkins, D. [1998]. *A short history of synthetic aperture sonar*. Proceedings, IEEE International Geoscience and Remote Sensing Symposium (IGARSS'98).

Groen, J.; Sabel, J.C.; and Htet, A. [2001]. *Synthetic aperture processing techniques applied to rail experiments with a mine hunting sonar*. Proceedings, Undersea Defence Technology Europe.

Jensen, F.B.; Kuperman, W.A.; Porter, M.B.; and Schmidt, H. [2011]. *Computational ocean acoustics*. Springer Science and Business Media. DOI: 10.1007/978-1-4419-8678-8.

King, P.; Venkatesan, R.; and Li, C. [2010]. *Modeling a shallow water acoustic communication channel using environmental data for seafloor sensor networks*. Wireless Communications and Mobile Computing, Vol. 10, No. 11, pp. 1521-1532. DOI: 10.1002/wcm.851.

Liptak, B.G. [2003]. *Instrument engineers' handbook, 4th edition, volume 1*. Process Measurement and Analysis, CRC Press. ISBN: 0849310830, 978-0849310836.

Lurton, X. [2002]. *An introduction to underwater acoustics: principles and applications*. Springer Science and Business Media. ISBN: 3540429670, 9783540429678.

Lynnworth, L.C. [2013]. *Ultrasonic measurements for process control: theory, techniques, applications*. Academic Press. ISBN: 0323138039, 9780323138031.

Munk, W.; Worcester, P.; and Wunsch, C. [2009]. Ocean acoustic tomography. Cambridge University Press. ISBN: 9780521115360.

NASA National Aeronautics and Space Administration [n.d.A]. *Ocean motion and surface currents: ship drift*. Retrieved from: http://oceanmotion.org/html/gatheringdata/shipdrift.htm.

NASA National Aeronautics and Space Administration [n.d.B]. *Ocean motion and surface currents*. Retrieved from: http://oceanmotion.org.

NOAA National Oceanic and Atmospheric Administration [n.d.A]. *Atlantic Oceanographic and Meteorological Laboratory*. Retrieved from: www.aoml.noaa.gov.

NOAA National Oceanic and Atmospheric Administration [n.d.B]. *Deep ocean drifter*. Retrieved from: http://oceanservice.noaa.gov/education/tutorial_currents/06measure4.html.

NOAA National Oceanic and Atmospheric Administration [n.d.C]. *Ocean surface current analyses – real time*. Retrived from: www.oscar.noaa.gov/index.html.

Paduan, J.D. and Graber, H. [1997]. *Introduction to high-frequency radar: reality and myth*. Oceanography, Vol. 10, No. 2, pp. 36-39.

Pandian, P.K.; Emmaneul, O.; Ruscoe, J.P.; Side, J.C.; Harris, R.E.; Kerr, S.A.; and Bullen, C.R. [2010]. *An overview of recent technologies on wave and current measurement in coastal and marine applications*. Journal of Oceanography and Marine Science, Vol. 1, No. 1, pp. 1-10.

Parallax [n.d.]. *XBee-PRO ZB S2B extended range module*. Retrieved from: www.parallax.com/product/32408.

Porter, M. [2011]. *The BELLHOP manual and user's guide*. Retrieved from: http://oalib.hlsresearch.com/Rays/HLS-2010-1.pdf.

Rossby, T. [2016]. *Visualizing and quantifying oceanic motion*. Annual Review of Marine Science, Vol. 8, pp. 35-57.

Shin, K. and Hammond, J. [2008]. *Fundamentals of signal processing for sound and vibration engineers*. John Wiley & Sons. ISBN: 978-0-470-51188-6.

Stefanov, A. and Stojanovic, M. [2011]. *Design and performance analysis of underwater acoustic networks*. IEEE Selected Areas in Communications, Vol.

29, No. 10, pp. 2012-2021.
Stojanovic, M. [2007]. *On the relationship between capacity and distance in an underwater acoustic communication channel.* ACM SIGMOBILE Mobile Computing and Communications Review, Vol. 11, No. 4, pp. 34-43.
Turnbull, I.D.; Fournier, N.; Stolwijk, M.; Fosnaes, T.; and McGonigal, D. [2015]. *Operational iceberg drift forecasting in Northwest Greenland*. Cold Regions Science and Technology, Vol. 110, pp. 1-18.
Urick, J.R. (1983). *Principles of underwater sound*. McGraw-Hill, New York. ISBN-13: 9780070660878.
WHOI Woods Hole Oceanographic Institution [n.d.]. *Moored profiler*. Retrieved from: www.whoi.edu/page.do?pid=8415&tid=3622&cid=10978.
Wille, P. [2005]. *Sound images of the ocean: in research and monitoring*. Springer Science and Business Media. DOI: 10.1007/3-540-27910-5.
Wilson, W.D.; Heitsenrether, R.; Gray, G.; Holcomb, N.; and Teng, C.-C. [2015]. *NOAA's recent field testing of current and wave measurement systems – part II*. Proceedings, IEEE/OES 11th Current, Waves and Turbulence Measurements, Florida, USA.
Zuckerman, S. and Anderson, S. [2014]. *Advances in passive remote sensing of ocean currents and depths*. IEEE International Geoscience and Remote Sensing Symposium IGARSS'2014.